Coupling the regional climate MAR model with the ice sheet model PISM mitigates the melt-elevation positive feedback

Alison Delhasse [1], Johanna Beckmann [2,3], Christoph Kittel [4,1], and Xavier Fettweis [1]

[1]Laboratory of Climatology, Department of Geography, SPHERES, University of Liège, Liège, Belgium
[2]Climate Impact Research (PIK), Member of the Leibniz Association, Potsdam, Germany
[3]Securing Antarctica's Environmental Future, Monash University, School of Earth, Atmosphere and Environment, Clayton, Australia
[4]Institut des Géosciences de l'Environnement (IGE), Université Grenoble Alpes/CNRS/IRD/G-INP, Grenoble, France

Correspondence to: Alison Delhasse (alison.delhasse@uliege.be)

Abstract. The Greenland Ice Sheet is a key contributor to sea level rise. By melting, the ice sheet thins, inducing higher surface melt due to lower surface elevations, accelerating the melt coming from global warming. This process is called the melt-elevation feedback and can be considered by using two types of models: atmospheric models, which can represent the surface mass balance (positive degree day, or polar-oriented regional climate models for instance). But these models generally use a fixed surface elevation. And on the other side, the ice sheet models represent the surface elevation evolution. The last ones do not represent the surface mass balance explicitly as well as polar-oriented regional climate models. A new coupling between the regional climate model MAR (Modèle Atmosphérique Régional) and the ice sheet model PISM (Parallel Ice Sheet Model) is presented here following the CESM2 (SSP5-8.5) scenario until 2100 at the MAR lateral boundaries. The coupling is extended to 2200 with a stabilised climate (+ 7 °C compared to 1961 – 1990) by randomly sampling the last 10 years of CESM2 to force MAR and reaches a sea level rise contribution of 64 cm. The fully coupled simulation is compared to a 1-way experiment where surface topography remains fixed in MAR. However, the surface mass balance is corrected for the melt-elevation feedback when interpolated on the PISM grid by using surface mass balance vertical gradients as a function of local elevation variations (offline correction). This method is often used to represent the melt-elevation feedback and prevents from a coupling too expensive in computation time. In the fully-coupled MAR simulation, the ice sheet morphology evolution (changing slope and reducing the orographic barrier) induces changes in local atmospheric patterns. More specifically, wind regimes are modified, as well as temperature lapse rates, which influences the melt rate through modification of sensible heat fluxes at the ice sheet margins. We highlighted mitigation of the melt lapse rate on the margins by modifying the surface morphology. The lapse rates considered by the offline correction are no longer valid at the ice sheet margins. If used (1-way simulation), this correction implies an overestimation of the sea level rise contribution of 2.5 %. The mitigation of the melt lapse rate on the margins can only be corrected by using a full coupling between an ice-sheet model and an atmospheric model.

1 Introduction

The mass balance (MB) of the Greenland Ice sheet (GrIS) is a key factor of the future estimation of sea level rise (SLR) (Oppenheimer et al., 2019). Among the components of the GrIS MB, changes in Surface Mass Balance (SMB) and iceberg discharge, surface meltwater runoff appears to be the main contributor to future SLR (Goelzer et al., 2013, 2020; Enderlin et al., 2014; Choi et al., 2021).

As a long-term consequence, the melting ice will also decrease the ice sheet topography. Such a thinning will influence the regional atmospheric circulation, particularly affecting the spatial distribution of precipitation (Vizcaíno et al., 2010). It will also enhance the surface melt through a positive feedback cycle since the lower elevation of the ice sheet surface results in stronger warming and melt (hereafter, melt-elevation feedback). Changes in topography are generally not considered in climate models, but they are in Ice Sheet Models (ISMs). In contrast, atmospheric models, especially Regional Climate Models (RCMs), can represent the atmospheric circulation, SMB and its components in a more realistic way than ISMs through the explicit resolution of physical polar processes involved in the interactions between the atmosphere and ice or snow surfaces. Therefore, the most optimal method to represent the melt-elevation feedback would be based on a coupling between a RCM and an ISM.

This kind of coupling has two main disadvantages. First, a RCM-ISM coupling is not trivial because the two types of models do not rely on the same spatial and temporal scales. Simulations of ice flow processes require relatively large time steps (of the order of one month) compared to those required for atmospheric dynamic resolution (of the order of one minute), which are significantly shorter. Conversely, ISMs are implemented on a finer grid (of the order of one kilometre) than RCMs (of the order of ten kilometres). These differences result in a high computational time for coupled simulations. Then depending on the ISM used in a RCM-ISM coupling, the response to climate change may be significantly different (Goelzer et al., 2013, 2020), while RCMs simulate relatively similar SMB for the same forcing (Fettweis et al., 2020). This means multiple couplings would be necessary between several ISMs and RCMs to quantify uncertainties.

An often-used alternative to coupling is to impose atmospheric conditions from an RCM on an ISM; either the ISM resolves an SMB based on the monthly mean temperature change (Robinson et al., 2011) or the SMB is directly imposed to the ISM (Goelzer et al., 2013). However, since the topography and ice mask are fixed in the RCM, this method does not consider the positive feedback between melt and elevation. In this case, it is possible to use vertical gradients as a function of local elevation variations (which implicitly takes into account the melt-elevation feedback) to correct the elevation-dependent MAR outputs for topographic variations simulated by the ISM (Franco et al., 2012; Helsen et al., 2012). ISMs can then use RCM-corrected outputs as direct inputs. This offline method is notably used in the Ice Sheet Model Intercomparison Project for CMIP6 (ISMIP6, Goelzer et al., 2020) exercise. Using an offline correction works well as long as SMB (particularly melt) is mainly influenced by the surface elevation through the temperature lapse rate. It could be limited once surface elevation changes affect synoptic circulation through modifications of precipitation patterns, for instance. Both methods have been compared in Le clec'h et al. (2019) by using GRISLI (ISM), and MAR (RCM) forced with MIROC5 (from CMIP5). They highlighted the need

for a coupling beyond 2100 due to the melt-elevation feedback and precipitation-circulation changes that cannot be correctly represented when using a simple offline correction as soon as the topography changes become significant.

As the coupling is dependent on the used ISM, we present a new coupling between the climate model MAR and the Parallel Ice Sheet Model (PISM) following an extremely warm scenario (CESM2 SSP5-8.5) until 2200. The coupling, explicitly considering the melt-elevation feedback, is compared to an alternative method of offline correction of the SMB to consider this feedback. First, the aim is (1) to analyse the evolution of the GrIS by 2200 with this new coupling following an extreme scenario. By comparing our coupled simulation with the 1-way experiment, we (2) assess the ability of the offline method to represent the melt-elevation feedback. We also highlight (3) which atmospheric feedbacks, and which physical processes, are influenced by the changes in surface topography.

Section 2 describes the methodology and different experiments used in the study. The first part of the result in Section 3.1 presents the GrIS evolution as simulated with our coupling until 2200. Section 3.2 compares 1-way and 2-way experiments by evidencing new negative feedback triggered by the evolving surface topography of the GrIS in the 2-way-coupling method. Results are discussed in Section 4 and we end by the conclusion in Section 5.

2 Data and methodology

2.1 Models

2.1.1 Regional climate model MAR

The MAR model is a hydrostatic regional climate model specially developed to represent polar climates. It is largely used over Greenland (Delhasse et al., 2020; Fettweis et al., 2020; Hofer et al., 2020; Fettweis et al., 2021) but also over Antarctica (Agosta et al., 2019; Kittel et al., 2020; Amory et al., 2021). The version 3.11.5 of MAR (MAR hereafter Fettweis et al., 2021) is used here at 25 km spatial resolution. For the coupling process, the important variables are SMB and surface temperature (ST), which are required as input by the ISM. These surface variables result from the interactions between the atmosphere and the first snow/ice layers of the ice sheet represented by the Surface-Ice-Snow-Vegetation-Atmosphere-Transfer (SISVAT) module in MAR. The good performance of MAR to simulate atmosphere/ice interactions, specifically near-surface temperature (Delhasse et al., 2020), is one of the keys to a successful coupling because it determines the two input variables used by the ISM (SMB and ST). Note that the MAR evaluation mention here use a version of MAR at 15 km of spatial resolution (Delhasse et al., 2020).

As MAR is a regional climate model, it needs lateral forcing fields every 6 hours to represent its own climate above the selected domain. We, therefore, selected one of the most climate-sensitive models (Hofer et al., 2020) among the CMIP6 models (CESM2) using the SSP5-8.5 scenario from the IPCC (Eyring et al., 2016; O'Neill et al., 2016; Riahi et al., 2017), and available when starting the study. The equilibrium climate sensitivity (a hypothetical value of global warming at equilibrium for a doubling of CO_2 relative to a 140-year period in the pre-industrial) of CESM2 is + 5.2 °C (mean of CMIP6: + 3.2 °C, Meehl et al., 2020). This choice was motivated by the aim of representing the worst (i.e. warmer) future scenario for the GrIS,

SSP5-8.5 being the most extreme scenario with an additional radiative forcing of 8.5 Wm^{-2} in 2100. The aim is to highlight the limits of both methods in representing the melt-elevation feedback in conditions of extreme warming.

CESM2 (SSP5-8.5, 6-hourly outputs) is currently only available until 2100. We extend our simulations to 2200 by forcing MAR with the last 10 years (2091 – 2100) of CESM2 sampled randomly over 2101 – 2200 (Table S1 in the Supplement). This means we apply a stabilised climate (mean conditions and interannual variability) to Greenland over 100 years. This extension of the large-scale forcing enables us to distinguish the effect of the rapidly increased warming projected with this scenario until 2100 compared to the effect of continued stable warming of + 7 °C above Greenland until 2200.

2.1.2 Ice Sheet Model PISM

To represent the dynamics and surface elevation of the Greenland Ice Sheet (GrIS), we utilise the Parallel Ice Sheet Model (PISMv1.2.1, called PISM hereafter), a high-resolution numerical ice-sheet/ice-shelf model (Bueler and Brown, 2009; Winkelmann et al., 2011). In PISM, the geometry, temperature, and basal strength of the ice sheet are incorporated into stress balance equations at each time step to determine the ice velocity. PISM employs two approximations for shallow ice sheets: the Shallow Ice Approximation (SIA) and the Shallow Shelf Approximation (SSA). The SIA is suitable for slowly flowing ice that deforms under its own weight, assuming a strong connection between the ice base and the bedrock. The softness of the ice, affecting its flow velocity, is modulated by an enhancement factor, which we set to $E = 3$ in our experiments. Faster flowing ice, such as ice streams, glaciers, and shelves, is approximated using the SSA. PISM combines both approximations into a hybrid stress balance mode (Bueler and Brown, 2009; Aschwanden et al., 2012). Basal sliding of the ice over the bedrock introduces basal resistance. The speed of basal sliding is determined by the sliding law, typically a power law relating to the basal shear stress and yield stress. In our study, we adopt the Mohr-Coulomb criterion and use an exponent of $q = 0.6$ for the sliding law. The model considers basal resistance based on the hypothesis that the ice sheet rests on a till layer. The yield stress represents the strength of this aggregate material at the base of an ice sheet. When yield stress is lower than the driving stress (d) there is likely to be sliding, and thus faster velocities can be observed. The driving stress in turn is dependent on the ice thickness (H) and surface gradients (Hs) of the ice: $d \propto Hs$. The thicker and steeper the ice, the higher the driving stress and most probably the ice velocity. The properties of the till are further approximated by using material properties such as the friction angle. We vary the till friction angle linearly between 5° and 40° with respect to bedrock elevation (between -700 m and 700 m), following Aschwanden et al. (2016). This variation in friction angle leads to lower friction at lower altitudes and below sea level, resulting in increased surface velocities at the margins of the ice sheet, thus improving the match of flow structure for the glaciers. To match the present-day extent of the ice sheet, we impose a strong negative surface mass balance at the margins of the Greenland present-day ice mask. This setup allows only for ice retreat in our experiments. We also enforce a minimum thickness of 50 m for floating ice at the calving front and utilise the von Mises calving law, which is suitable for glaciers in Greenland (Morlighem et al., 2016). All other parameters are set to default values (University of Alaska Fairbanks, 2019). Our simulations do not consider bedrock deformation or changes in ice-ocean interaction, as we maintain constant submarine melt rates.

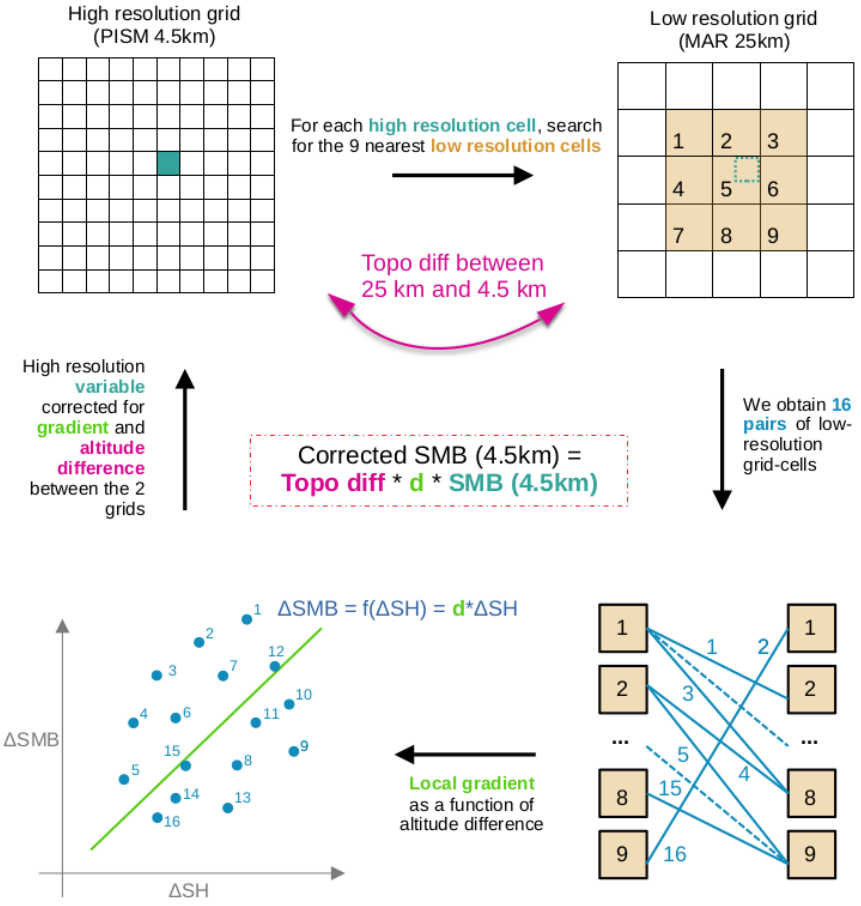

Figure 1. Steps of the offline correction as described in Franco et al. (2012). After interpolation of a variable (SMB, surface mass balance, in this figure) from a low to higher resolution grid, this variable is corrected to consider the influence of the temperature lapse rate with altitude. The correction is based on a local gradient (d) calculated by considering SMB differences (ΔSMB) between 9 nearest grid cells in the neighbourhood of the current one in the source grid in function of the surface elevation difference (ΔSH). Modified from Wyard (2015).

2.1.3 Inisialisation of PISM

PISM is forced by yearly ST and SMB from MAR forced by CESM2. To achieve a stable spinup state, we forced PISM with the MAR mean fields (ST and SMB) over 1961 – 1990, when the GrIS was close to balance (Fettweis et al., 2017). However, for a realistic thermodynamics representation of the ice sheet, the temperature evolution of the last glacial cycle has to be considered, because the surface temperature slowly propagates down the ice column and determines the vertical ice profile of the ice sheet. The ice profile determines the ice softness and deformability, thus affecting the flow velocity of the ice.

For a glacial spinup, it is assumed that the state of the ice sheet before a glacial cycle is equal to the one at present day, which means that ice topography and surface temperatures are as well. However, different surface topographies lead to different surface temperatures (which we achieve during our coupled spinup runs). This is why it is common practice to use temperature anomalies over the last glacial cycle, because the assumption of equal glacial states before and after the glacial cycle only holds when using anomalies.

Thus the first model initialisation (Fig. 2) was run over 125 000 years with a scalar temperature anomaly of the 2D-temperature mean field of 1961 – 1990. The historical time series (Johnson et al., 2019) includes the temperature derived from Oxygen Isotope Records from the Greenland Ice Core Project (GRIP, Johnson et al., 2019). We followed the grid refinement defined by Aschwanden et al. (2016) for computational efficiency. Starting in SIA-only mode, and an 18 km grid at -125 000 years, we refined our grid to 9 km at -25 000 years and to 4.5 km at -5000 years. For the last -1000 years, we kept the resolution fixed but added the SSA to the SIA stress regime to represent better the fast-flowing outlet glaciers.

2.2 Coupling method

The coupling between both models has been performed by exchanging yearly outputs (SMB and ST from MAR, and ice thickness from PISM) on the 1st January of each year for 1991 – 2200 as described in Le clec'h et al. (2019). For MAR, this induces updating the surface elevation and ice extent of the ice sheet at the beginning of each year with PISM results from the previous year, whereas SMB and ST are used as forcing fields for PISM.

Before any data exchange between the models, data has to be interpolated on the destination grid because the two models were run at two different spatial resolutions (25 vs 4.5 km). The surface elevation simulated by PISM is then aggregated using a four-nearest-neighbour distance-weighted method on the MAR grid at 25 km. The MAR variables are interpolated using the same method on the PISM grid at 4.5 km. However, they are further corrected by considering the difference in altitude between the two grids at the time of interpolation thanks to local vertical SMB/ST gradients. This method is described in Franco et al. (2012) and is called offline correction hereafter. Firstly, a linear and elevation-dependent gradient (Fig. 1) is calculated over the MAR grid by considering the values of the considered variable (SMB at 4.5 km in our example, Fig. 1) of the eight surrounding grid cells of the current one. This gradient is specific to each PISM grid cell and is locally determined. An example of this gradient can be found in Fig. S1 in the Supplement. Subsequently, these gradients are utilised to correct the variable when it is interpolated onto the PISM grid. The correction is performed by multiplying the interpolated variable by the gradient and the difference in surface elevation between the grid cells in MAR and in PISM. This offline correction is specifically employed to correct variables that are influenced by temperature lapse rate with altitude, namely temperature and derived variables.

2.3 Simulations

2.3.1 Initialisation of the coupling

The coupling requires initialisation to achieve an equilibrium state between the two models over a reference period (1961 – 1990). Successive forcings of each model by the other one should produce similar results to the previous iteration over the

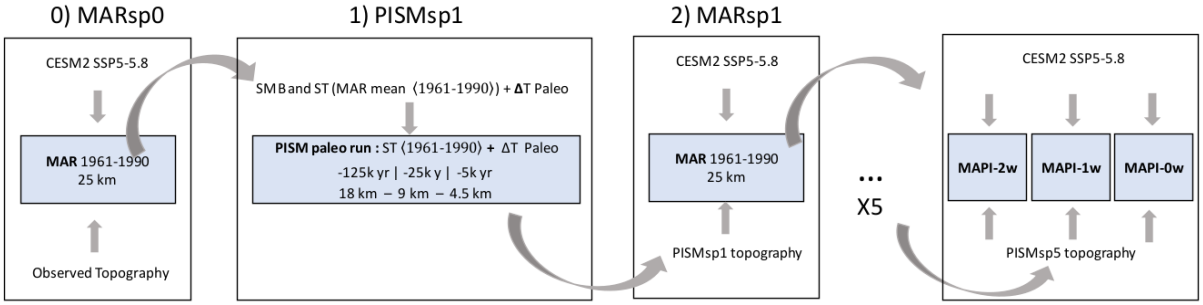

Figure 2. Steps of the coupling initialisation. Each MAR step corresponds to a 30-year long run over the reference period (1961-1990). And each PISM step consists of a new initialisation cycle of PISM as described in Section 2.3.1.

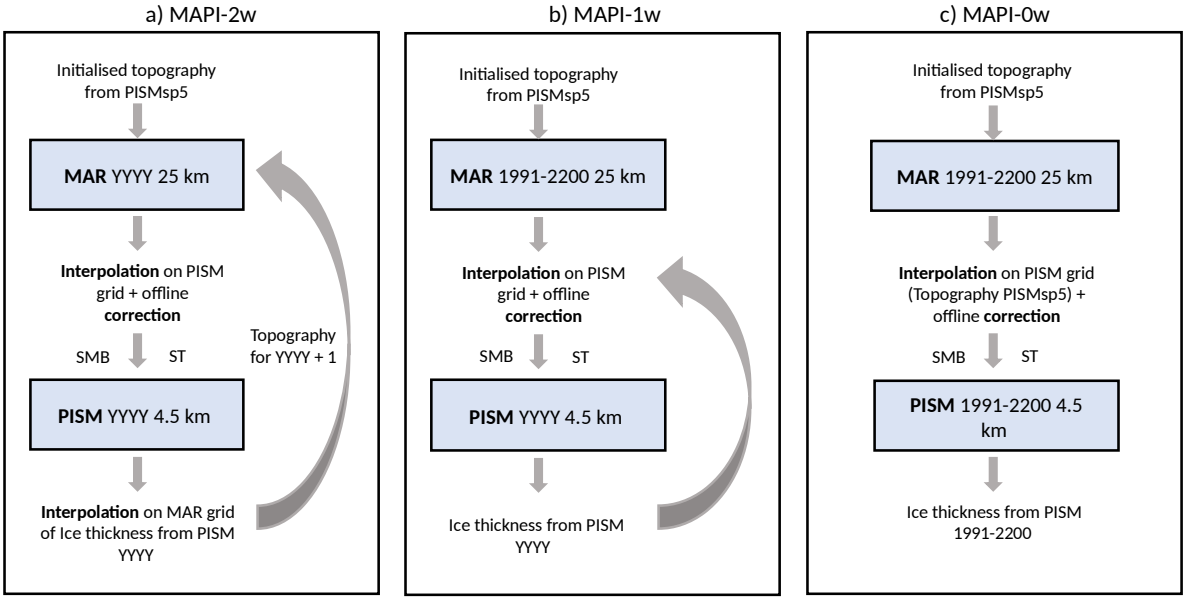

Figure 3. Coupling details for a) 2-way, b) 1-way and c) 0-way experiments.

same reference period (Fig. 2). These simulations are called spinup hereafter. In practical terms, we firstly forced PISM using the SMB and ST climatology of MAR 1961 – 1990 (MARsp0, based on the observed topography and ice mask, and CESM2 as a large-scale forcing field, Howat et al., 2014, 2017) and temperature anomalies of the last glacial cycle (see Section 2.1.3) resulting in a first equilibrium state (PISMsp1). This method assumes that the ice sheet topography before the last glacial cycle was similar to the preindustrial one and reiterates this process should correct for errors in ice thickness. The next step (MARsp1) consists in running MAR using the new ice extent and topography from PISMsp1 over the same period (still 1961 –

1990). The corrected surface topography (PISMsp1) together with the corrected SMB and ST climatology (MARsp1) are the new base to re-start our initialisation over a whole glacial cycle, as described in Section 2.1.3. The new surface topography, PISMsp2, is then used to derive the new climatological mean field of (1961 – 1990) with MAR (MARsp2). We repeated these successive forcings (5 iterations are needed here) until both models reached an equilibrium state regardless of the new forcing. This means that differences between the two spinup stages no longer influence the other model (Fig. S1 in the Supplement).

The PISMsp5 topography, the last step of the initialisation process, will be the initial state of the different simulations compared here and is used to run the MAR reference simulation over the reference period (MARref). As our projections could not be evaluated, we evaluated the performances of MARref over the present. To do so, we compared MAR results over the current period (1961 – 1990), with the initialised topography (PISMsp5) forced on one hand, by the Earth System Model used for projections (CESM2) and on the other hand ERA5 reanalysis (Hersbach et al., 2020), considered as observations and well representing the current climate. The main point of this evaluation is that MARref is significantly colder than MAR forced by ERA5 in the south of Greenland, but this bias does not significantly influence SMB results (See Fig. S3 in the Supplement). It is due to the cold bias of CESM2 compared to reanalyses (Hofer et al., 2020).

The ice sheet topography and velocity field of the PISMsp5 final run and their difference to observational data sets are depicted in the Supplement (Fig. S4). The ice sheet thickness of the final spinup is overestimated up to 150 m in the northeast and southwest of the GrIS. In comparison, the northwest and central west are underestimated up to 200 m compared to the observational data set (Fig. S4a). As there is no complete observational velocity data set from 1961 to 1990, we, therefore, compare it with the complete velocity data set by Joughin et al. (2018), which gives the average velocities from 1995 to 2015. Our comparison shows a general agreement of the velocity pattern with an average difference between modelled and observed ice speeds of $\pm$ 80 $\mathrm{m\,yr^{-1}}$ on the margins (Fig. S4b). In some fast-flowing glacier regions, differences are well larger. However, the coarse resolution (4.5 km) compared to the proximity of smaller glaciers (500 m), which are solved by the observations, lead to strong deviation in their comparison.

2.3.2 Coupled simulation

The first simulation is the 2-way experiment which consists of a coupled simulation of MAR and PISM called MAPI-2w hereafter. We started to run MAR in 1991 with the PISMsp5 topography forced with CESM2 (Fig. 3a). At the end of this first year, we interpolated SMB and ST on the PISM grid with the offline correction. Then, PISM is running for the same year and produces a new ice thickness that will further be aggregated onto the MAR grid to start the following year (i.e. 1992) with an updated topography. When the MAR topography is updated, we also update the ice mask in function of PISM ice extent. The melt-elevation feedback is, therefore, explicitly taken into account by the MAPI-2w simulation through an evolving topography in MAR.

2.3.3 Uncoupled simulations

The 1-way experiment (called MAPI-1w hereafter) consists in a simulation where MAR is running with PISMsp5 topography (built over the reference period) for 1991 – 2200 without any more interaction from PISM to MAR (Fig. 3b). Then we inter-

polated the yearly results of SMB and ST from MAR to the PISM grid with the offline correction. Thus, the new PISM input variables were corrected for changes in the surface height of the evolving ice sheet topography of PISM compared to the fixed MAR surface elevation. The MAPI-1w experiment considers then the melt-elevation feedback a posteriori through the offline correction, meaning that it is not explicitly solved by any of the two models (MAR or PISM), nor are the implied physical processes. As MAR is evolving alone, no update on the ice mask has been done. To be consistent, we consider the smallest ice mask all along the analyses, meaning the one in 2200 of the MAPI-2w simulation, to compare both simulations.

We also consider a PISM simulation forced with MAR-fixed-topography corrected over the initial PISM topography (PISMsp5). This experiment is called the MAPI-0w experiment (Fig. 3c) hereafter due to its non-consideration of the melt-elevation feedback.

2.4 Representation of the results

The coupling aims to produce estimations of total MB of the GrIS by simulating dynamical components directly with PISM and using the SMB components as simulated by MAR as forcing for PISM.

For the sake of consistency of the results, we decided to present all results on the PISM grid, whether they are PISM or MAR outputs. The MAR variables used in the analyses below are therefore interpolated on the PISM grid. While those from the coupled simulation explicitly include the influence of melt-elevation feedback, the variables from the uncoupled simulation (MAPI-1w) are corrected offline during the interpolation. This correction is applied to the variables dependent on the surface elevation influence, i.e., temperature, SMB, meltwater production and runoff. On the other hand, the following variables will not be corrected during their interpolation since they do not depend on the evolution of the surface elevation: total precipitation (snowfall and rainfall) and wind. However, some comparisons have been carried out on the MAR grid, but this is well specified each time.

The two main PISM simulations, which are compared hereafter (MAPI-2w and -1w), evolve independently and consequently have differences in surface topography. These differences (Fig. S5 in the Supplement) are only responsible for 10 % of the MB differences between two experiments in 2200 (Fig. S6 in the Supplement) and will be further neglected. Throughout the analysis, we will consider the MAR results interpolated on the MAPI-2w coupled PISM grid (4.5 km) regardless if they are from MAR coupled or uncoupled simulation.

3 Results

3.1 Coupled MB and SMB

This section is exclusively dedicated to describing changes in total mass balance, surface mass balance and its components in the future as simulated with the 2w-coupling experiment compared to the reference period.

Our results project a fast increase in annual mass loss for an extreme warming rate (Fig. 4). It corresponds to a contribution to sea level rise of 16 cm in 2100 (total loss of ice mass since 1991 of > 50 x10^3 Gt) for a global warming of + 7 °C in 2100

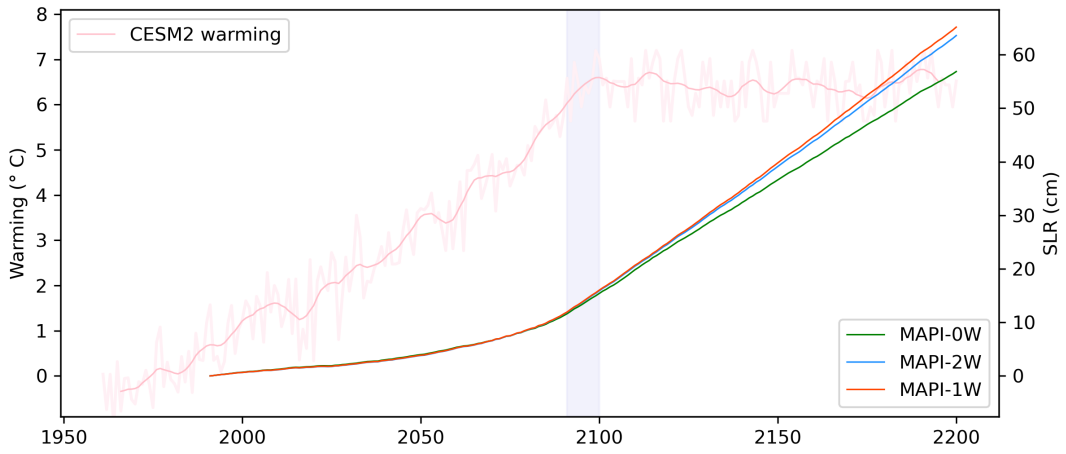

Figure 4. Contribution to sea level rise (SLR, cm) of the Greenland Ice Sheet according to MAR-PISM 2-way (in blue),) 1-way (in red) and 0-way (in green) experiments. In pink is the corresponding warming (°C) applied in the MAR lateral boundaries following CESM2 SSP5-8.5 (mean temperature at 600 hPa over Greenland). The last 10 years of CESM2 randomly sampled until 2200 to extend the CESM2-forcing of MAR are in grey.

(+ 6.8 °C on average for 2091 – 2100) compared to our reference period (1961 – 1990). After 2100 this warming is stabilised (+ 7 °C on average for 2101-2200), the ice sheet continues to lose mass, and the sea level rise contribution reaches 64 cm (total loss of ice mass since 1991 of > 200 x10^3 Gt). Since there is an acceleration of the warming and consequently of the mass loss before 2100, even by stabilising the climate and then the warming after 2100, the mass loss is still increasing until 2200.

Whereas the GrIS is retreating by a few kilometres all around its margins (Fig. 5), extremely negative cumulated mass balance (MB) in 2200 results in a decrease in surface elevation of several hundred metres at the GrIS margins. The western margin is more affected by the mass loss and, thus, the decrease in elevation. Many peripheral glaciers seem to disappear by 2200, especially in the east and north of the island.

The SMB decrease largely drives the increase in mass loss. To attribute the individual factors of the SMB loss, we examine the native 25 km output MAR-2w (Fig. 6 solid lines). The SMB evolution is marked by an accelerated decrease after 2050 to 2100 and a slowdown from 2100 to 2200 when the climate stabilises again. The changes in SMB are dominated by runoff (RU hereafter) resulting from larger meltwater production (ME hereafter) not refreezing into the snowpack.

Due to global warming, we expect more precipitation. Combined with the lower surface elevation, we also expect more liquid precipitation. The snowfall (SF) evolution remains constant until the end of the simulation (Fig. 6). The slight increase in total precipitation is mainly due to increased rainfall (RF). Surprisingly, only a short part of RF increase (1 % when comparing RF from MAR coupled, solid lines, and uncoupled, dashed lines) is caused by the decrease in surface elevation, which converts more SF into RF.

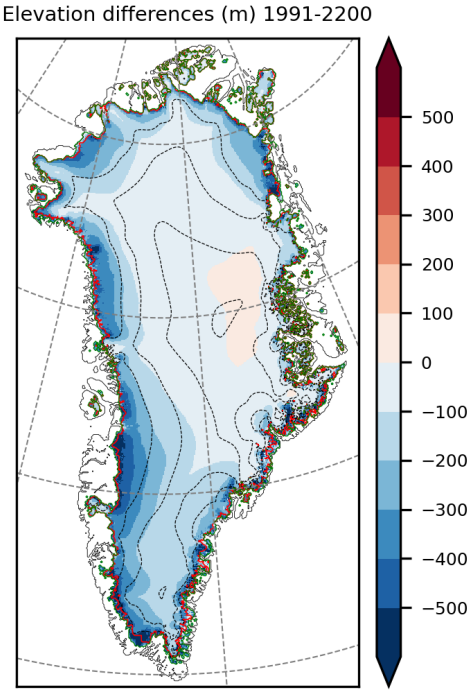

Figure 5. Surface elevation changes (m) as simulated by the 2-way coupling between MAR and PISM between 1991 and 2200. In green, the ice extent as in 1991 and in red as in 2200.

The spatial distribution of the SMB component changes is explained mainly by the warming of the scenario and emphasised by the decrease in surface elevation until 2200 (Fig. 7a). ME and RU (Fig. 7e and f), which drive the spatial pattern of the SMB (Fig. 7d), are projected to occur more inland. For instance, almost the entire southern half of Greenland is affected by RU in 2200. This results in a SMB decrease in these regions triggering changes in surface topography, evidencing the dependence of the MB on the SMB.

While total precipitation over Greenland does not appear to change significantly (Fig. 6), its spatial distribution does change with topography compared to the reference period in the coupled simulation. There is a significant decrease in total precipitation (SF + RF, Fig. 7c) over the southeast due to synoptic features of the large-scale forcing (CESM2, not shown). Conversely, our simulation projects significantly increase over the west and north of Greenland. The increase in the west is a consequence of the ice sheet thinning as clouds can penetrate more inland due to a weaker topographic barrier effect and a delayed condensation due to further lift-up of air masses. A synoptic pattern coming from the CESM2 forcing is also contributing to this increase in precipitation (not shown). We attribute changes in snowfall for the north of Greenland to more humidity content associated with atmospheric warming, as this region is particularly dry and cold over present-day conditions. This results in a slight increase when integrating the precipitation over the whole ice sheet, mainly due to an increase in RF resulting from global warming and

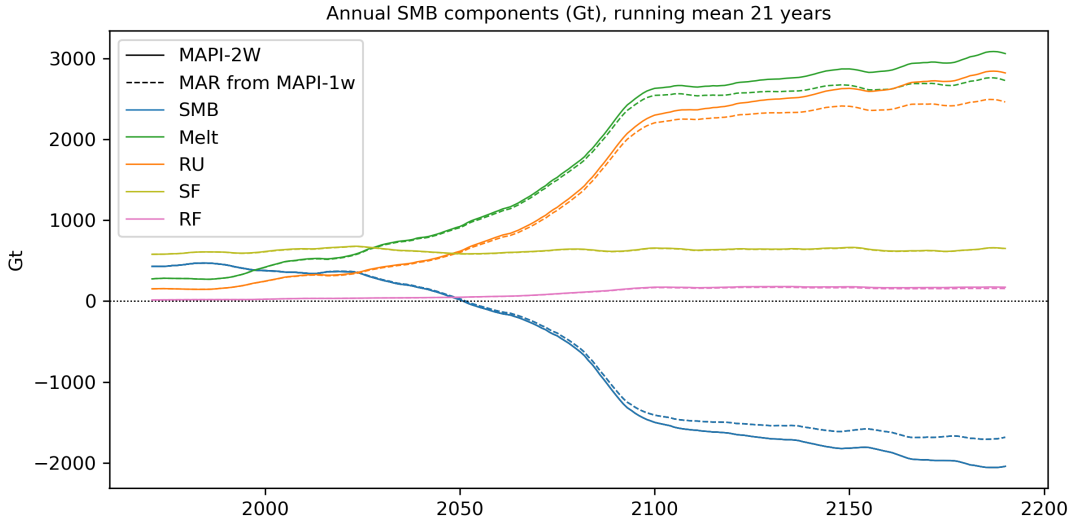

Figure 6. Surface mass balance (SMB, in blue), Meltwater production (ME, in green), meltwater Runoff (RU, in orange), Snowfall (SF in yellow) and Rainfall (RF, in pink) evolution (in Gt) as simulated by MAR 2-way coupled with PISM (MAPI-2w, solid lines) from 1991 to 2200. Dotted lines are corresponding evolution as simulated by MAR uncoupled (MAPI-1w).

changes in surface elevation, as explained before. However, significant changes in the spatial distribution of precipitation do not influence the global pattern of SMB since runoff changes are far larger.

The decreased mass loss of the ice sheet is accompanied by an overall speedup of the ice dynamics inland and a slow down at the margins (Fig. 8a). Surface velocity relates to the driving stress, and the spatial pattern of driving stress changes (Fig. 8b) mainly explains the spatial pattern of changes in surface velocities. As the driving stress relates to the product of ice thickness and surface slope, the pronounced thinning at the margins of the ice explains the reduction in driving stress in these regions. While there is also an increase in surface slope at the margins, which would increase the driving stress, the thinning is of larger importance and determines the reduction in driving stress. Although less pronounced than in the margins, the ice interior still experiences an increase in surface slope. Further inland, the increase in surface slope emphasises the driving stress as the thinning is smaller than the thinning at the margins. Therefore the increased driving stress leads there to higher surface velocities.

The overall pattern of speedup in the ice interior and slow down at the margins is observed in the 2-way and 1-way experiments. However, in MAPI-2w, ice thickness is slightly larger at the margins and thinner in the ice interior than in MAPI-1w. At the margins, this reduces the surface slope and, compared to the 1-way experiment, leads to slower velocities (Fig. S5b in the Supplement).

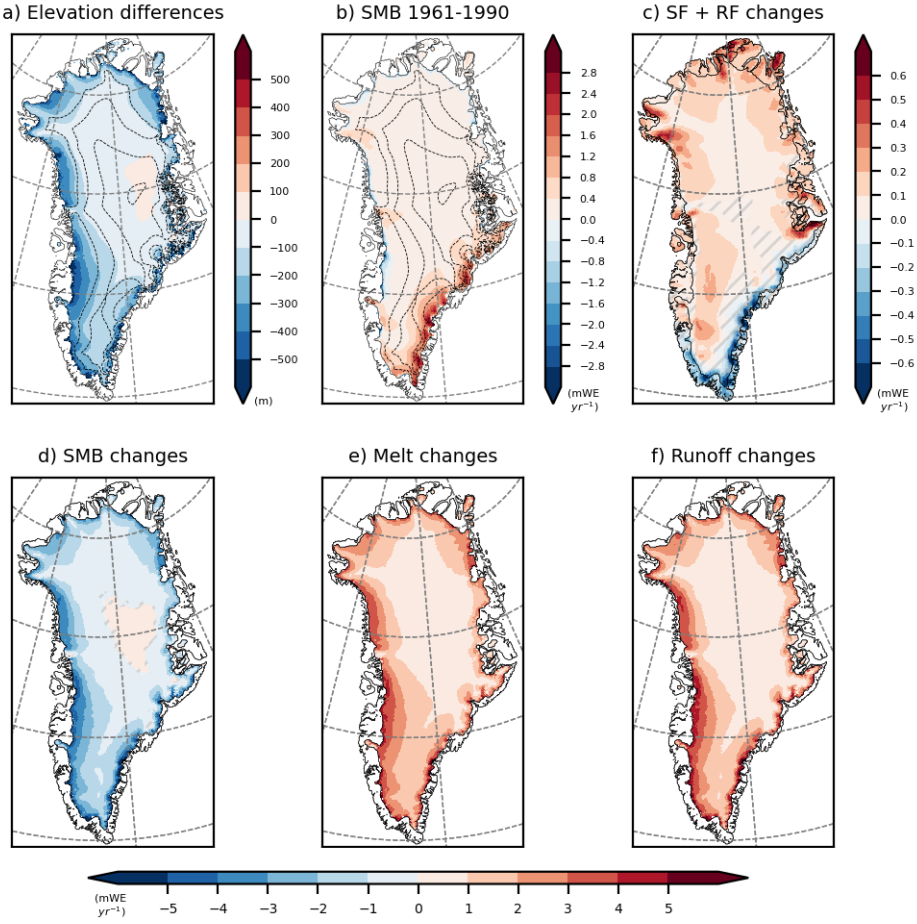

Figure 7. a) Surface elevation changes (m) between 1991 and 2200 as simulated by the MAR-PISM 2-way coupling (MAPI-2w). b) Surface mass balance (SMB, mWE yr^{-1}) for the reference period (1961 – 1990) as simulated by MAPI-2w. c) Precipitation (snowfall, SF and rainfall, RF, mWE yr^{-1}), d) SMB (mWE yr^{-1}), e) Meltwater production (mWE yr^{-1}) and f) meltwater Runoff (mWE yr^{-1}) changes in 2171 – 2200 compared to the reference period. Non-significant changes are hatched (smaller than the interannual variability of the reference period).

3.2 Comparison of coupled and uncoupled experiments

This section focuses on the differences in the results obtained by the two methods of considering the melt-elevation feedback (MAPI-1w vs MAPI-2w).

Comparing the total mass loss in 2200 (Fig. 4), the different strategies in representing the melt-elevation feedback (MAPI-1w vs MAPI-2w) do not result in a significantly-different total mass loss in 2200. Total ice loss is 229 x10^3 Gt with MAPI-2w and 234 x10^3 Gt with MAPI-1w, meaning that MAPI-1w overestimates the SLR contribution of 2.5 % (1.6 cm) compared to MAPI-2w. MAPI-0w largely underestimates ice loss by 10.5 % (6.7 cm less of SLR than MAPI-2w) due to its non-representation of the melt-elevation feedback. These three experiments start to diverge when the climate is stabilised.

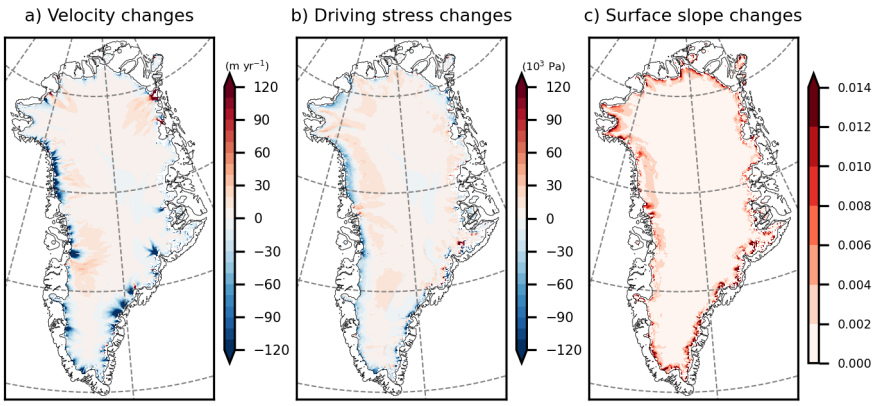

Figure 8. Changes (2200 – 1990) in a) velocity (m yr^{-1}), b) driving stress (10^3 Pa) and c) surface slope of the coupled MAR-PISM simulation (MAPI-2w).

The MB overestimation by MAPI-1w could be contrary to the intermediate results from MAR of both MAPI-1w and -2w simulations. If we look at these results (raw MAR outputs) before interpolation and forcing of PISM, fully-coupled melt rate outputs are higher than in the one-way coupled simulation (Fig. 6 dashed lines). After interpolation, meaning the MAR results interpolated on PISM-grid and which actually forced PISM (Fig. 6 solid lines), MAPI-1w gave higher melt rates than MAPI-2w. This highlights that when we correct the SMB for melt-elevation feedback by the offline correction (MAPI-1w on PISM grid), the SMB becomes exaggeratedly negative compared to the 2-way coupling, which explicitly considers this feedback. It is in opposition to (Le clec'h et al., 2019) as discussed later.

The corrected SMB provided to PISM in both MAPI-1w and MAPI-2w differ significantly on the margin of the ice sheet (Fig. 9a), indicating a greater mass loss for MAPI-1w. The different SMB components are analysed here (Fig. 9) to identify what causes this underestimation of the MAPI-1w-corrected SMB. Firstly, whether on the east or west coast, there is a different distribution of total precipitation when simulated by MAPI-2w compared to MAPI-1w (Fig. 9f). Precipitation falls more inland (positive differences) in the coupled mode since the slope is flattened, but this is not significant compared to the annual variability (2171 – 2200 standard deviation). Therefore, this does not explain the SMB differences in the margins between the two simulations. The main driver is the meltwater runoff (Fig. 9b) resulting from the ME excess (Fig. 9e) not refreeze in the snowpack. ME depends on the sensible heat flux (SHF) related to air temperature and wind speed which are also overestimated on the margins by MAPI-1w (Fig. 9d and e).

The underestimation of SMB in MAPI-1w is due to an overestimation of the melt-elevation feedback by the offline correction when interpolating MAPI-1w towards the PISM grid compared to the explicit consideration of this feedback in MAPI-2w. This correction is based on the linear temperature dependence with the surface elevation to account for the melt-elevation feedback that alters the SMB and related variables. The correction applies local linear gradients according to these altitude differences. We compare, on the MAR grid, the yearly evolution of the altitude differences between the two experiments (coupled and uncoupled) with the evolution of the temperature differences inside the ice sheet and on the margin (Fig. 10a).

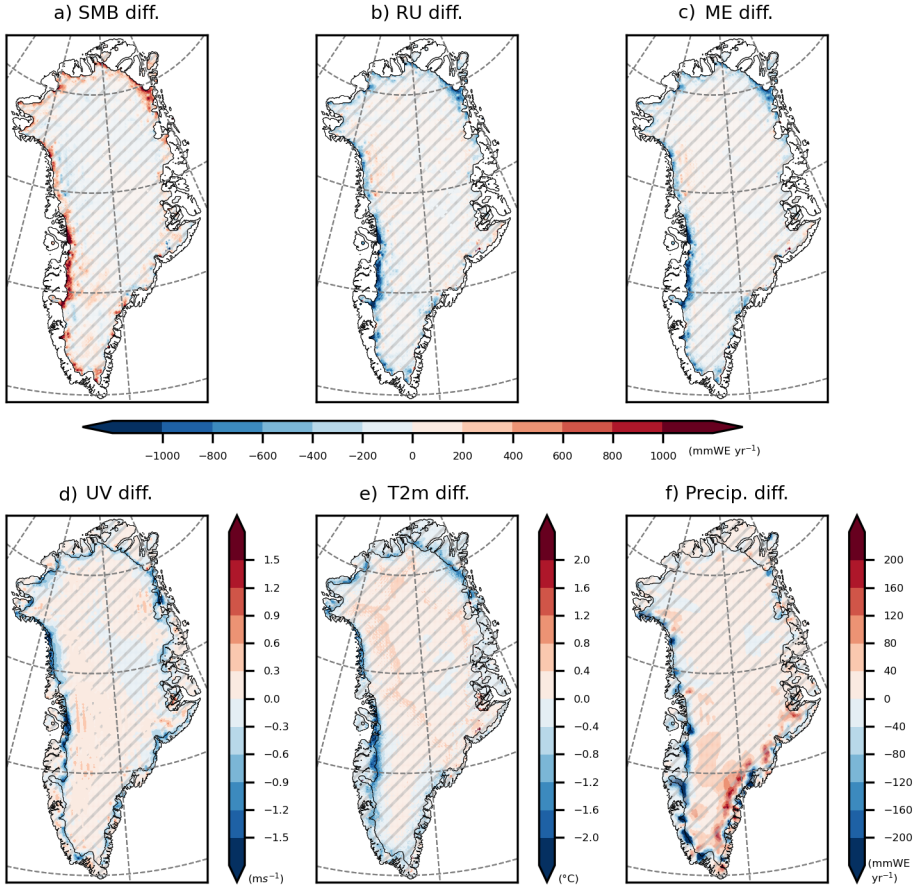

Figure 9. Differences (2w minus 1w) of a) SMB (mmWE yr^{-1}), b) Runoff (RU, mmWE yr^{-1}), c) meltwater production (ME, mmWE yr^{-1}), d) 10m-wind speed (UV, ms^{-1}), e) 2m-temperature (T2m, °C), and f) total precipitation (Precip. are the sum of rainfall and snowfall) between the MAPI-2w and MAPI-1w simulations for 2171 – 2200. Insignificant differences are hatched (smaller than the interannual variability of 2171-2200).

We notice that on the margin, differences in altitude between the two MAR-grid (ΔSH) explain only 61% (69% for melt) of the changes in temperature differences (ΔT2m and ΔME respectively), compared with the interior of the ice-sheet where these relationships are much more dependent, with R^2 of 0.99 and 0.94 respectively. In our example (Fig. 10a), modifications of the topography in the 2-way coupling experiment have modified this linear relationship with the temperature from -0.4 °C/100m inside to -0.1 °C/100m. The same relationships are illustrated for melt differences (Fig. 10b), confirming the modification in linear dependence with changes in surface elevation. We will now compare these gradients, obtained by comparing the MAR simulations with and without changes to the topography over time, with the gradients used by the offline correction. These are calculated locally, i.e. taking into account the differences in altitude and in the variable considered with the surrounding

grid cells. For the example of the temperature, we find gradients of -0.69 and -0.65 °C/100m in 2200 respectively for the same locations as in Fig. 10 inside the ice sheet and on the margins. Although in absolute values these gradients are different from those obtained by comparing the two simulations over time, the difference between the two regions is smaller. The gradient applied to the margin of the ice sheet follows a similar dependency to that of the interior of the ice sheet. This explains the exaggeration of temperature and temperature-dependent variables (melt, SMB, etc.) on the margins by the correction, given the use of a gradient that is too large and does not reflect processes leading to the mitigation of the temperature altitude dependence, and consequently, melt-elevation feedback. Finally, we can note hat beyond a 350 m drop in altitude, the association between changes in altitude and temperature (or melting) at the ice margin exhibits a distinct behavior, resembling the relationship observed within the ice sheet. Further confirmation is required through experiments involving larger elevation variations that exceed those explored in our current simulation. All these comparisons highlight two main elements: (1) the linear-offline correction of SMB is no longer valid in the ice sheet margins; (2) the changes in the linear-relationship between temperature and altitude driving the melt-elevation feedback lead to mitigation of this feedback along the ice sheet margins.

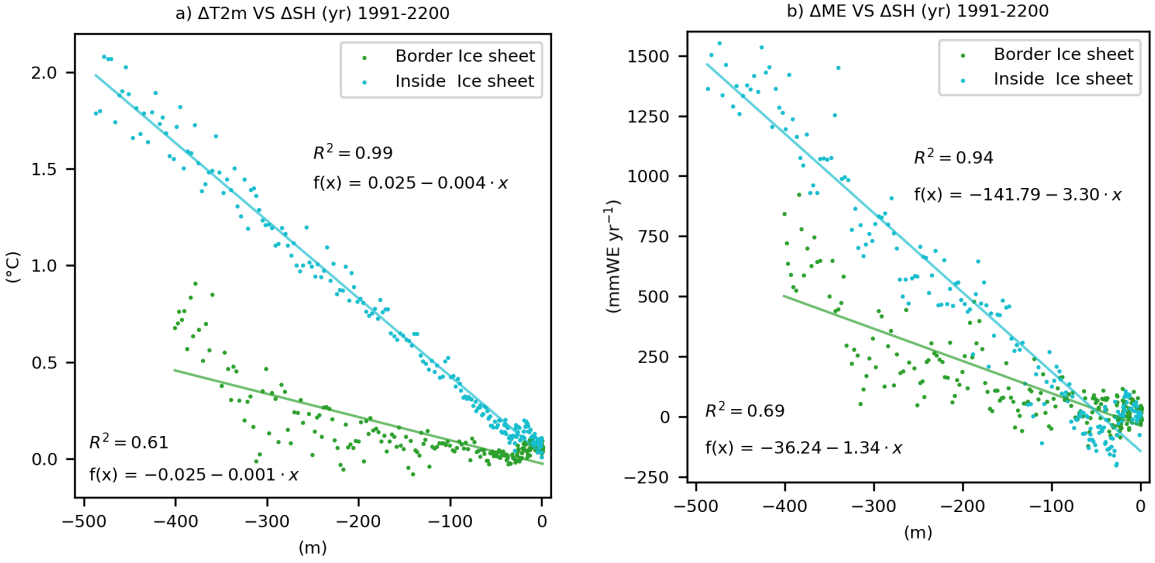

Figure 10. Association of the yearly (1991 – 2200) differences on MAR grid in surface elevation (ΔSH, m) with a) differences in 2m-temperature (ΔT2m, °C) and b) meltwater production (ΔME, mmWE yr^{-1}) between coupled (MAPI-2w) and uncoupled (MAPI-1w) simulation for a MAR grid cell (25 km) inside the ice sheet (49.26 ° W, 67.05 ° N, in blue) and one at the boundary with the tundra (48.83 ° W, 67.05 ° N in green). These grid cells are located on the same section of the West Greenland than in Fig. 11. Regressions are presented in the respective colours.

The mitigation of the melt-elevation feedback in the MAR-coupled simulation is explained by the modification of the local wind and temperature patterns near the margins around the GrIS. The evolution of the topography in the coupled simulation

(for instance, Fig. 11e) causes a decrease in the melt increase with the elevation lowering. The production of meltwater is the result of a positive energy balance at the surface. More specifically, changes in sensible heat flux (SHF) account for this which is directly proportional to surface temperature and wind speed. We investigate here differences in these two parameters between the two experiments. They are both directly influenced by changes in surface topography between MAPI-2w and -1w (Fig. 11b and d). The near-surface temperature, as well as the north-south wind component, are altered along the margin, specifically in the west part of the GrIS in the fully-coupled simulation (general wind speed, as well as west-east wind component differences, are presented in the Supplement, Fig. S7). To better illustrate that, we compare the vertical temperature and wind speed patterns above both simulation topographies along a transect crossing the ice sheet. The example illustrated in Fig. 11 highlights that the north-south wind component (v-wind, positive northward) is larger in the uncoupled simulation on the grid cell on the ice sheet margin (inside the ice sheet, Fig. 11c and d). Secondly, the mean near-surface temperature that appears on the 2200-topography (coupled MAR) on the same grid cell of the ice sheet margin is lower than the temperature computed on the uncoupled MAR topography while at a lower altitude (Fig. 11a and b). Changes in wind and temperature in the MAR-coupled simulation explain the weaker melt increase with elevation lowering.

The temperature changes and (v)-wind speed decrease in the coupled MAR simulation compared to the uncoupled one could be explained by local modifications of the wind regime and of the margin morphology that mitigate the surface melt. In general, Fig. 11a shows a greater amount of warm air at the edges of the ice sheet in the uncoupled simulation, as the original topography acts as a wall preventing air from entering at depth. In the coupled simulation, warm air can penetrate further the ice sheet and dissipate, without greatly increasing melting. On the other hand, in actual conditions, barrier winds occur when air masses from the tundra cross the ice sheet, which acts as an orographic barrier (Van den Broeke and Gallée, 1996). These winds induce warm air advection from the tundra (warmer than the surrounding air of the ice sheet) locked by the orographic barrier and leading to northward wind (on the west coast) along the ice sheet margin. They lead to high melt events due to increased wind speed and higher temperatures along the ice sheet margins. As the orographic barrier is weakened by the thinning and retreat of the ice sheet (Fig. 11e) in MAPI-2w compared to MAPI-1w, the barrier winds could be reduced as suggested by the decrease in the v-wind component (south-north) in the coupled experiment. This further would create differences in temperature between the two experiments as less warm air advection can occur due to the weaker barrier wind in MAPI-2w. This would have an impact on the local gradient of melt/temperature with surface elevation and would lead to a mitigation of melt in MAPI-2w compared to MAPI-1w where the barrier winds remain unnaffacted as the topography does not change.

4 Discussion

The feedback between topography and local atmospheric circulation highlighted here adds uncertainty to the SLR projections, which are already affected by uncertainties related to the ice dynamics modelling. For instance, in ISMIP6, SLR estimations vary from 6.5 to 13.5 cm in 2100 for the same climate forcing (MAR forced by MIROC5 using the RCP8.5 scenario) with the different ISMs and experiments (Goelzer et al., 2020). ISMIP6 experiments can be compared to our MAPI-1w simulation

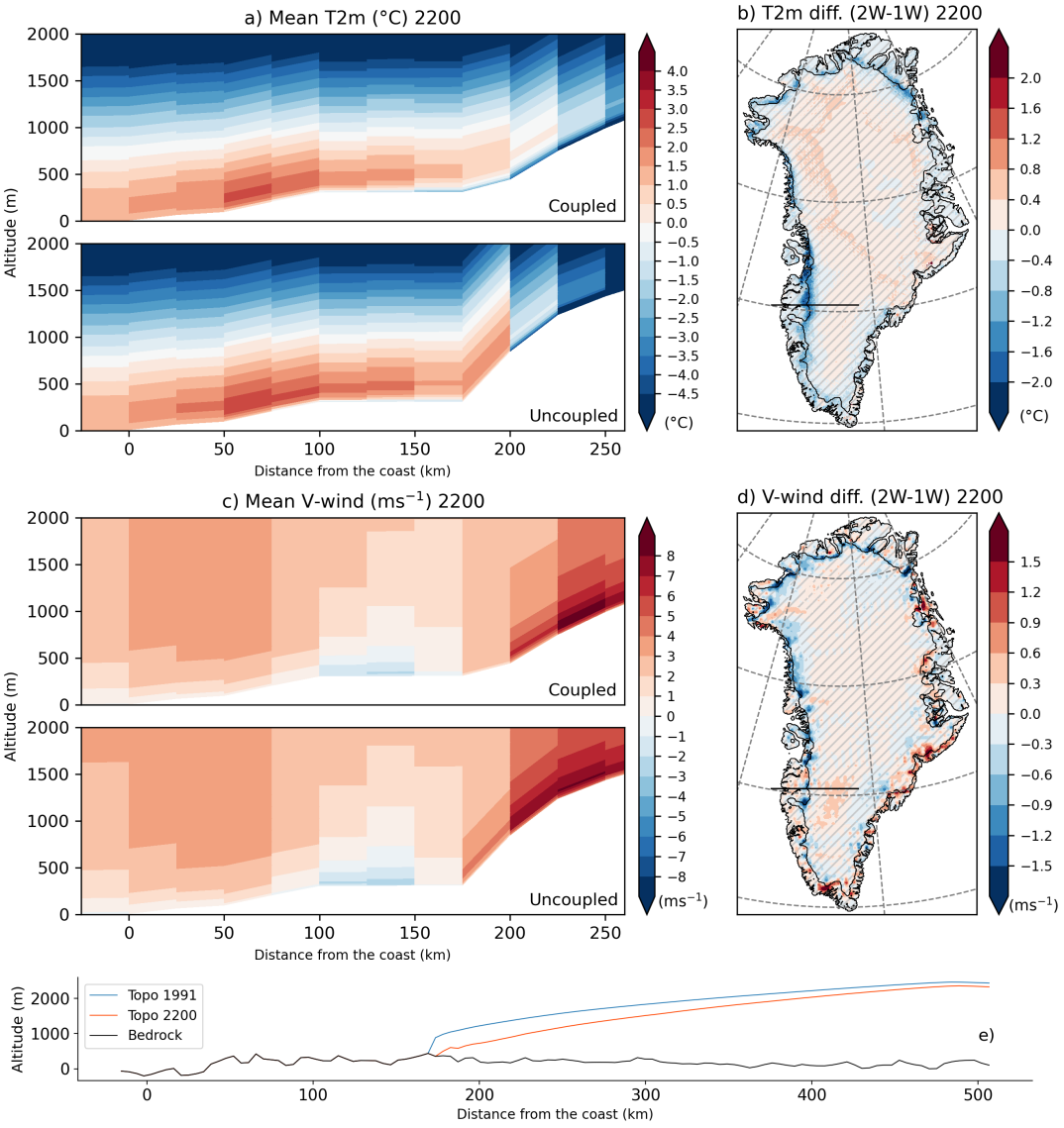

Figure 11. Cross sections along 66.64–67.35 ° N of a) temperature (T2m, °C) and c) V-wind component (north-south, positive northward, ms^{-1}) on the MAR grid for the coupled (above) and the uncoupled (below) simulation. Differences in b) 2m-temperature (°C) and d) V-wind component (ms^{-1}) between 2-way and 1-way experiments of MAR and PISM (MAPI-2w - MAPI-1w) in 2200. Non-significant differences (lower than the interannual variability over 2171 – 2200) are hatched. T2m and V-wind are interpolated in PISM grid (b and d) to be consistent with other figures, T2m is corrected with the offline correction but not the V-wind as it is not related to surface elevation. e) Cross section along black lines in b) and d) on the west coast of the PISM grid (similar to the cross-section in a) and c) subplots) on MAR grid 66.64–67.35 ° N) of the surface elevation (m) of the MAPI-2w in 2200 (in red), in 1991 in blue (fixed topography in MAR for MAPI-1w simulation) and the bedrock in black.

because their methodology uses MAR outputs corrected offline of the melt-elevation feedback. Such a method could be compromised to extend simulations due to uncertainties added by the varying topography of the ice sheet and its interaction with the near-surface climate discussed in this study.

Le clec'h et al. (2019) present the closest methodology of coupling to ours. They used MAR and GRISLI to represent GrIS until 2150. Besides the ISM used, the main difference in their study is the large-scale forcing field to force MAR (i.e. MIROC5, a CMIP5 model using the RCP8.5 scenario). As the future climate of MIROC5 is not as warm as CESM2 (difference of $+1.5\,^{\circ}\mathrm{C}$, Hofer et al., 2020), SLR contributions are consequently well higher by using CESM2. The 2100 warming of MIROC5 is already reached in 2080 for CESM2. Concerning their 2-way coupled simulation, given the difference in warming applied to the coupling (MIROC5 RCP8.5 vs CESM2 SSP5-8.5), their MB results in 2100 are similar to those of MAPI-2w in 2080. From the dynamical point of view, the overall pattern of speedup in the ice interior and slowdown at the margins of the GrIS towards the end of the simulation is as well observed in their study as in ours.

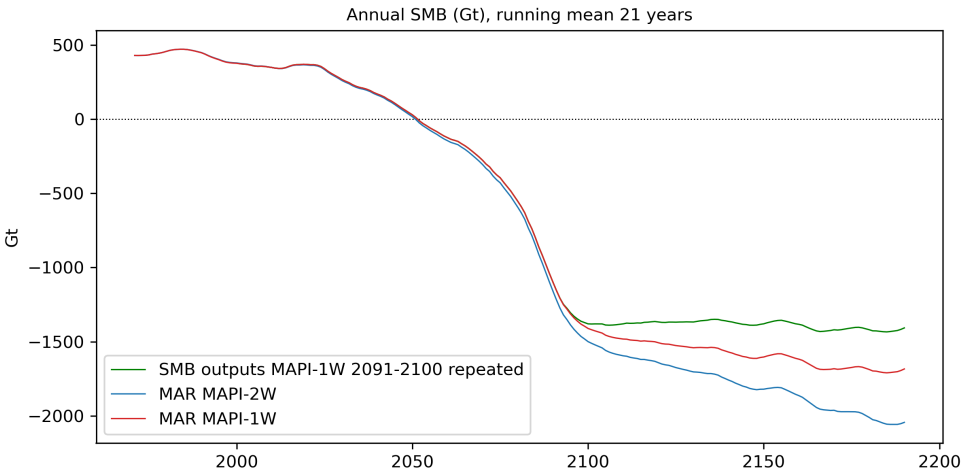

Figure 12. Yearly surface mass balance (SMB) integrated over all the ice sheet as simulated by MAR uncoupled (no update of the topography, in red), by MAR coupled (topography updated each year, in blue) and by MAR uncoupled until 2100 and last 10 years of SMB outputs repeated until 2200 (in green).

However, after 2100 they used constant MAR outputs (SMB and ST) to force GRISLI and extend their 1-way simulation until 2150 without continuing to run MAR on the fixed topography. By doing this, they assume that with a stable climate (no more warming), SMB becomes directly stable. To extend our MAPI-1w simulation beyond 2100, we decided to repeat the last 10 years of large-scale forcing randomly to run MAR until 2200 to allow time for snowpack to stabilise with the new warm stabilised climate over 2101 – 2200. The main difference with Le clec'h et al. (2019) is that after 2100, our MAR simulations using a fixed topography were still running with repeated CESM2 forcing fields. In contrast, in their corresponding simulation, MAR did not run beyond 2100. We compare our 1-way and 2-way experiment results with a simulation where the last 10 years of MAR from MAPI-1w outputs (same 10-years as CESM2-repeated ones) were directly used to force PISM and extend

MAPI-1w simulation from 2100 until 2200 without running MAR anymore (SMB outputs 2091 – 2100 repeated, similar to the Le clec'h et al. (2019) method of the 1-way experiment). It appears that in MAPI-1w, SMB is well decreasing for decades compared to repeated MAR-fixed outputs (Fig. 12). This demonstrates that even without additional warming, the ablation area is still growing after 2100. The snowpack transforms from an accumulation to an ablation state in a larger part of the ice sheet. It needs decades to be stabilised before reaching a stable state of meltwater retention capacity. As shown in the RetMIP exercise (Retention Model Intercomparison, Vandecrux et al., 2020), the required time to stabilise the meltwater retention capacity is very likely model-dependent due to parameters such as the maximum liquid water enabled in the snowpack and the considered-snowpack height. This study also highlights that SMB (through runoff) cannot be considered stable as soon as the warming is stopped. During the snowpack response time, the meltwater saturates deep layers, and it becomes warmer and denser, leading to a decrease in its capacity to retain meltwater. When the snowpack reaches its maximum retention capacity, it transforms into impermeable firn or bare ice. Due to the method used in extending the 1-way simulation, this process is neglected in Le clec'h et al. (2019). Our respective comparison of the method to represent the melt-elevation feedback (1-way VS 2-way coupling) is then not comparable, as it does not have a common physical basis.

Another significant aspect of our method under discussion relates to the spatial resolution of the MAR model. To reach a balance between computational efficiency and adequately representing the SMB within the ensemble, we opted for a relatively coarse spatial resolution of 25 km. At the scale of the entire GrIS, this resolution proves to be a viable choice for capturing the global SMB evolution, as supported by previous research (e.g. Fettweis et al., 2020). However, at a finer scale of analysis, this resolution may compromise the accurate representation of local wind and temperature patterns. In some cases, a grid point might span an area as large as the ablation zone, introducing potential inaccuracies (Van de Wal et al., 2012; Hermann et al., 2018). RCMs remain sensitive to horizontal resolution, particularly when aiming to accurately represent SMB and Surface Energy Balance (SEB) in specific areas. The local representation of processes and surface topography by the model plays a crucial role in this sensitivity (Franco et al., 2012; van de Berg et al., 2020).

5 Conclusions

The coupling of the RCM MAR and the ISM PISM is presented here following the SSP5-8.5 scenario as simulated by CESM2. The 2-way coupling is compared to a 1-way and a 0-way (uncoupled) experiment to evaluate the importance of the melt-elevation feedback.

The first aim was to study what became GrIS in 2200 by applying such extreme conditions. Our coupling simulation projects a contribution of 64 cm to SLR by 2200 with a stabilised climate since 2100 of + 7 °C compared to our reference period (1961 – 1990). Until 2100 our results are comparable with results obtained in other studies (e.g., Goelzer et al., 2020).

The most effective approach for representing melt-elevation feedback involves fully coupling an atmospheric model with an ice sheet model. Neglecting this feedback leads to an underestimation of the projected sea-level rise contribution by 10.5 %. When comparing two methods to account for the melt-elevation feedback (coupling and offline correction), we highlight that

the corrected SMB from the MAR model underestimates the coupled-SMB by 2.5 % when interpolated on the PISM grid using this correction.

The offline correction is no longer valid on the ice sheet margins because it fails to consider the mitigation of temperature lapse rates and, consequently, melt due to changes in topography, such as retreat and slope alterations. These changes influence the wind regime at the margins of the MAR-coupled simulation. The mitigation of melt rates depends on the reduction of sensible heat flux due to changes in local wind regimes and temperature lapse rates. A hypothesis to explain these local changes around the ice sheet margins involves modifications of barrier wind regimes. These winds typically act along the ice sheet, transporting warmer air from the tundra, enhancing the surface melt, and increasing the northward wind speed along the west side, for instance. The orographic barrier, crucial for the formation of such winds, diminishes with the evolving topography in MAPI-2w. Consequently, enhanced melt could be mitigated, as well as melt-elevation feedback. However, fruther investigation is required to validate this assumption and to understand the underlying physical processes responsible for these local wind regime changes initiated by modified surface topography in a warmer climate. A moment budget comparing both simulations (MAPI-1w and -2w) could help identify differences in local atmospheric circulation patterns leading to such variations in representing melt rates at the margins (van Angelen et al., 2011). Additionally, a complete analysis focusing on characteristics such as recurrence and synoptic situations favourable to the development of these wind events will be necessary to gain a better understanding of the physical processes involved. In conclusion, the coupling is essential to update the surface topography in the RCM and to consider all interactions between the near-surface atmosphere and the new morphology.

By extending our simulations beyond the available period of large-scale forcing of MAR (CESM2), we highlighted that assuming SMB stability when climate conditions become stable is not valid. It is essential to consider the response time of the snowpack to warming rates and its capacity to retain meltwater. Conducting further sensitivity tests will be necessary to determine if the response time of the ice sheet in stabilising the snowpack depends on the parameterisation of snow layer conditions, such as the maximum liquid water content in a layer or the height of the snowpack simulated by the model.

In conclusion, our study emphasises the significance of topography in influencing the local atmospheric pattern, particularly in shaping local wind regimes along the ice sheet margins, in addition to the well-known melt-elevation feedback. Since these processes influence melt in opposite ways, the melt-elevation feedback is mitigated by the evolving topography. This aspect is not accounted for in the commonly used offline correction, which aims to avoid computationally time-consuming coupling between climate and ice sheet models to perform MB projections and to consider the melt-elevation feedback. Neglecting this negative feedback leads to an overestimation of 2.5 % (1.6 cm) in the SLR contribution compared to the result obtained with full coupling. Such oversight introduces uncertainty in projections (e.g. ISMIP project) that fail to consider this process, which can be accurately represented through an atmosphere-dynamics coupling.

Author contributions. AD and JB conceived the study. AD and JB performed the simulations. AD led the writing of the manuscript. AD, JB, CK and XF discussed the results. All co-authors revised and contributed to the editing of the manuscript.

Competing interests. The authors have the following competing interests: Xavier Fettweis is an editor of The Cryosphere.

Acknowledgements.

References

Agosta, C., Amory, C., Kittel, C., Orsi, A., Favier, V., Gallée, H., van den Broeke, M. R., Lenaerts, J., van Wessem, J. M., van de Berg, W. J., and Fettweis, X.: Estimation of the Antarctic surface mass balance using the regional climate model MAR (1979-2015) and identification of dominant processes, The Cryosphere, 13, 281–296, https://doi.org/10.5194/tc-13-281-2019, 2019.

Amory, C., Kittel, C., Le Toumelin, L., Agosta, C., Delhasse, A., Favier, V., and Fettweis, X.: Performance of MAR (v3. 11) in simulating the drifting-snow climate and surface mass balance of Adélie Land, East Antarctica, Geoscientific Model Development, 14, 3487–3510, https://doi.org/10.5194/gmd-14-3487-2021, 2021.

Aschwanden, A., Bueler, E., Khroulev, C., and Blatter, H.: An enthalpy formulation for glaciers and ice sheets, Journal of Glaciology, 58, 441–457, https://doi.org/10.3189/2012JoG11J088, 2012.

Aschwanden, A., Fahnestock, M. A., and Truffer, M.: Complex Greenland outlet glacier flow captured, Nature Communications, 7, 10 524, https://doi.org/10.1038/ncomms10524, 2016.

Bueler, E. and Brown, J.: Shallow shelf approximation as a "sliding law" in a thermomechanically coupled ice sheet model, Journal of Geophysical Research: Solid Earth, 114, 1–21, https://doi.org/10.1029/2008JF001179, 2009.

Choi, Y., Morlighem, M., Rignot, E., and Wood, M.: Ice dynamics will remain a primary driver of Greenland ice sheet mass loss over the next century, Communications Earth & Environment, pp. 1–9, https://doi.org/10.1038/s43247-021-00092-z, 2021.

Delhasse, A., Christoph, K., Amory, C., Hofer, S., and Fettweis, X.: Brief communication: Interest of a regional climate model against ERA5 to simulate the near-surface climate of the Greenland ice sheet, The Cryosphere, 137, 957–965, https://doi.org/10.5194/tc-14-957-2020, 2020.

Enderlin, E. M., Howat, I. M., Jeong, S., Noh, M. J., Van Angelen, J. H., and Van Den Broeke, M. R.: An improved mass budget for the Greenland ice sheet, Geophysical Research Letters, 41, 866–872, https://doi.org/10.1002/2013GL059010, 2014.

Eyring, V., Bony, S., Meehl, G. A., Senior, C. A., Stevens, B., Stouffer, R. J., and Taylor, K. E.: Overview of the Coupled Model Intercomparison Project Phase 6 (CMIP6) experimental design and organization, Geoscientific Model Development, 9, 1937–1958, https://doi.org/10.5194/gmd-9-1937-2016, 2016.

Fettweis, X., Box, J., Agosta, C., Amory, C., Kittel, C., Lang, C., van As, D., Machguth, H., and Gallée, H.: Reconstructions of the 1900–2015 Greenland ice sheet surface mass balance using the regional climate MAR model, The Cryosphere, 11, 1015–1033, https://doi.org/10.5194/tc-11-1015-2017, 2017.

Fettweis, X., Hofer, S., Krebs-Kanzow, U., Amory, C., Aoki, T., Berends, C. J., Born, A., Box, J. E., Delhasse, A., Fujita, K., Gierz, P., Goelzer, H., Hanna, E., Hashimoto, A., Huybrechts, P., Kapsch, M.-L., King, M. D., Kittel, C., Lang, C., Langen, P. L., Lenaerts, J. T. M., Liston, G. E., Lohmann, G., Mernild, S. H., Mikolajewicz, U., Modali, K., Mottram, R. H., Niwano, M., Noël, B., Ryan, J. C., Smith, A., Streffing, J., Tedesco, M., van de Berg, W. J., van den Broeke, M., van de Wal, R. S. W., van Kampenhout, L., Wilton, D., Wouters, B., Ziemen, F., and Zolles, T.: GrSMBMIP: intercomparison of the modelled 1980–2012 surface mass balance over the Greenland Ice Sheet, The Cryosphere, 14, 3935–3958, https://doi.org/10.5194/tc-14-3935-2020, 2020.

Fettweis, X., Hofer, S., Séférian, R., Amory, C., Delhasse, A., Doutreloup, S., Kittel, C., Lang, C., Van Bever, J., Veillon, F., and Ivrine, P.: Brief communication: Reduction in the future Greenland ice sheet surface melt with the help of solar geoengineering, The Cryosphere, 15, 3013–3019, https://doi.org/10.5194/tc-15-3013-2021, 2021.

Franco, B., Fettweis, X., Lang, C., and Erpicum, M.: Impact of spatial resolution on the modelling of the Greenland ice sheet surface mass balance between 1990–2010, using the regional climate model MAR, The Cryosphere, 6, 695–711, https://doi.org/10.5194/tc-6-695-2012, 2012.

Goelzer, H., Huybrechts, P., Fürst, J. J., Nick, F. M., Andersen, M. L., Edwards, T. L., Fettweis, X., Payne, A. J., and Shannon, S.: Sensitivity of Greenland ice sheet projections to model formulations, Journal of Glaciology, 59, 733–749, https://doi.org/10.3189/2013JoG12J182, 2013.

Goelzer, H., Nowicki, S., Payne, A., Larour, E., Seroussi, H., Lipscomb, W. H., Gregory, J., Abe-Ouchi, A., Shepherd, A., Simon, E., Agosta, C., Alexander, P., Aschwanden, A., Barthel, A., Calov, R., Chambers, C., Choi, Y., Cuzzone, J., Dumas, C., Edwards, T., Felikson, D., Fettweis, X., Golledge, N. R., Greve, R., Humbert, A., Huybrechts, P., Le Clec'H, S., Lee, V., Leguy, G., Little, C., Lowry, D., Morlighem, M., Nias, I., Quiquet, A., Rückamp, M., Schlegel, N. J., Slater, D. A., Smith, R., Straneo, F., Tarasov, L., Van De Wal, R., and Van Den Broeke, M.: The future sea-level contribution of the Greenland ice sheet: A multi-model ensemble study of ISMIP6, The Cryosphere, 14, 3071–3096, https://doi.org/10.5194/tc-14-3071-2020, 2020.

Helsen, M. M., Van De Wal, R. S. W., Van Den Broeke, M. R., Van De Berg, W. J., and Oerlemans, J.: Coupling of climate models and ice sheet models by surface mass balance gradients: Application to the Greenland Ice Sheet, The Cryosphere, 6, 255–272, https://doi.org/10.5194/tc-6-255-2012, 2012.

Hermann, M., Box, J. E., Fausto, R. S., Colgan, W. T., Langen, P. L., Mottram, R., Wuite, J., Noël, B., van den Broeke, M. R., and van As, D.: Application of PROMICE Q-transect in situ accumulation and ablation measurements (2000–2017) to constrain mass balance at the southern tip of the Greenland Ice Sheet, Journal of Geophysical Research: Earth Surface, 123, 1235–1256, 2018.

Hersbach, H., Bell, B., Berrisford, P., Hirahara, S., Horányi, A., Muñoz-Sabater, J., Nicolas, J., Peubey, C., Radu, R., Schepers, D., Simmons, A., Soci, C., Abdalla, S., Abellan, X., Balsamo, G., Bechtold, P., Biavati, G., Bidlot, J., Bonavita, M., De Chiara, G., Dahlgren, P., Dee, D., Diamantakis, M., Dragani, R., Flemming, J., Forbes, R., FUentes, M., Geer, A., Haimberger, L., Healy, S., Hogan, R. J., Hólm, E., Janisková, M., Keeley, S., Laloyaux, P., Lopez, P., Lupu, C., Radnoti, G., De Rosnay, P., Rorum, I., Vamborg, F., Vollaume, S., and Thépaut, J.-N.: The ERA5 global reanalysis, Quarterly Journal of the Royal Meteorological Society, https://doi.org/10.1002/qj.3803, 2020.

Hofer, S., Lang, C., Amory, C., Kittel, C., Delhasse, A., Tedstone, A., and Fettweis, X.: Greater Greenland Ice Sheet contribution to global sea level rise in CMIP6, Nature communications, 11, 1–11, https://doi.org/10.1038/s41467-020-20011-8, 2020.

Howat, I., Negrete, A., and Smith, B.: MEaSUREs Greenland Ice Mapping Project (GIMP) Digital Elevation Model from GeoEye and WorldView Imagery, Version 1 [Data Set], https://doi.org/10.5067/H0KUYVF53Q8M, last access 09-15-2022, 2017.

Howat, I. M., Negrete, A., and Smith, B. E.: The Greenland Ice Mapping Project (GIMP) land classification and surface elevation data sets, The Cryosphere, 8, 1509–1518, https://doi.org/10.5194/tc-8-1509-2014, 2014.

Johnson, J., Hand, B., and Bocek, T.: Greenland Standard Data Set, Available online at http://websrv.cs.umt.edu/isis/index.php/Present_Day_Greenland (last access: 1 August 2023), 2019.

Joughin, I., Smith, B. E., and Howat, I. M.: A complete map of Greenland ice velocity derived from satellite data collected over 20 years, Journal of Glaciology, 64, 1–11, https://doi.org/10.1017/jog.2017.73, 2018.

Kittel, C., Amory, C., Agosta, C., Jourdain, N. C., Hofer, S., Delhasse, A., Doutreloup, S., Huot, P.-V., Lang, C., Fichefet, T., and Fettweis, X.: Diverging future surface mass balance between the Antarctic ice shelves and grounded ice sheet, The Cryosphere Discussions, pp. 1–29, https://doi.org/10.5194/tc-15-1215-2021, 2020.

Le clec'h, S., Charbit, S., Quiquet, A., Fettweis, X., Dumas, C., Kageyama, M., Wyard, C., and Ritz, C.: Assessment of the Greenland ice sheet–atmosphere feedbacks for the next century with a regional atmospheric model coupled to an ice sheet model, The Cryosphere, 13, https://doi.org/10.5194/tc-13-373-2019, 2019.

Meehl, G. A., Senior, C. A., Eyring, V., Flato, G., Lamarque, J.-F., Stouffer, R. J., Taylor, K. E., and Schlund, M.: Context for interpreting equilibrium climate sensitivity and transient climate response from the CMIP6 Earth system models, Science Advances, 6, 1–10, https://doi.org/10.1126/sciadv.aba198, 2020.

Morlighem, M., Bondzio, J., Seroussi, H., Rignot, E., Larour, E., Humbert, A., and Rebuffi, S.: Modeling of Store Gletscher's calving dynamics, West Greenland, in response to ocean thermal forcing, Geophysical Research Letters, 43, 2659–2666, 2016.

O'Neill, B. C., Tebaldi, C., van Vuuren, D., Eyring, V., Friedlingstein, P., Hurtt, G., Knutti, R., Kriegler, E., Lamarque, J.-F., Lowe, J., Meehl, G. A., Moss, R., Riahi, K., and Sanderson, B. M.: The Scenario Model Intercomparison Project (ScenarioMIP) for CMIP6, Geoscientific Model Development, 9, 3461–3482, https://doi.org/10.5194/gmd-9-3461-2016, 2016.

Oppenheimer, M., Glavovic, B., Hinkel, J., van de Wal, R., Magnan, A., Abd-Elgawad, A., Cai, R., Cifuentes-Jara, M., DeConto, R., Ghosh, T., Hay, J., Isla, F., Marzeion, B., Meyssignac, B., and Z., S.: Sea Level Rise and Implications for Low-Lying Islands, Coasts and Communities, in: IPCC Special Report on the Ocean and Cryosphere in a Changing Climate, edited by Pörtner, H.-O., Roberts, D., Masson-Delmotte, V., Zhai, P., Tignor, M., Poloczanska, E., Mintenbeck, K., Alegría, A., Nicolai, M., Okem, A., Petzold, J., Rama, B., and Weyer, N., 2019.

Riahi, K., van Vuuren, D. P., Kriegler, E., Edmonds, J., O'Neill, B. C., Fujimori, S., Bauer, N., Calvin, K., Dellink, R., Fricko, O., Lutz, W., Popp, A., Cuaresma, J. C., KC, S., Leimbach, M., Jiang, L., Kram, T., Rao, S., Emmerling, J., Ebi, K., Hasegawa, T., Havlik, P., Humpenöder, F., Da Silva, L. A., Smith, S., Stehfest, E., Bosetti, V., Eom, J., Gernaat, D., Masui, T., Rogelj, J., Strefler, J., Drouet, L., Krey, V., Luderer, G., Harmsen, M., Takahashi, K., Baumstark, L., Doelman, J. C., Kainuma, M., Klimont, Z., Marangoni, G., Lotze-Campen, H., Obersteiner, M., Tabeau, A., and Tavoni, M.: The Shared Socioeconomic Pathways and their energy, land use, and greenhouse gas emissions implications: An overview, Global Environmental Change, 42, 153–168, https://doi.org/10.1016/j.gloenvcha.2016.05.009, 2017.

Robinson, A., Calov, R., and Ganopolski, A.: Greenland ice sheet model parameters constrained using simulations of the Eemian Interglacial, Climate of the Past, 7, 381–396, https://doi.org/10.5194/cp-7-381-2011, 2011.

University of Alaska Fairbanks: Parallel Ice Sheet Model, GitHub [code], Available online at https://github.com/pism/pism/releases/tag/v1.1.3 (last access: 1 August 2023), 2019.

van Angelen, J. H., Van den Broeke, M., and Van de Berg, W.: Momentum budget of the atmospheric boundary layer over the Greenland ice sheet and its surrounding seas, Journal of Geophysical Research: Atmospheres, 116, 2011.

van de Berg, W. J., van Meijgaard, E., and van Ulft, L. H.: The added value of high resolution in estimating the surface mass balance in southern Greenland, The Cryosphere, 14, 1809–1827, 2020.

Van de Wal, R., Boot, W., Smeets, C., Snellen, H., Van den Broeke, M., and Oerlemans, J.: Twenty-one years of mass balance observations along the K-transect, West Greenland, Earth System Science Data, 4, 31–35, 2012.

Vandecrux, B., Mottram, R., Langen, P. L., Fausto, R. S., Olesen, M., Stevens, C. M., Verjans, V., Leeson, A., Ligtenberg, S., Kuipers Munneke, P., Marchenko, S., van Pelt, W., Meyer, C. R., Simonsen, S. B., Heilig, A., Samimi, S., Marshall, S., Machguth, H., MacFerrin, M., Niwano, M., Miller, O., Voss, C. I., and Box, J. E.: The firn meltwater Retention Model Intercomparison Project (RetMIP): evaluation of nine firn models at four weather station sites on the Greenland ice sheet, The Cryosphere, 14, 3785–3810, https://doi.org/10.5194/tc-14-3785-2020, 2020.

Vizcaíno, M., Mikolajewicz, U., Jungclaus, J., and Schurgers, G.: Climate modification by future ice sheet changes and consequences for ice sheet mass balance, Climate Dynamics, 34, 301–324, https://doi.org/10.1007/s00382-009-0591-y, 2010.

Winkelmann, R., Martin, M. A., Haseloff, M., Albrecht, T., Bueler, E., Khroulev, C., and Levermann, A.: The Potsdam Parallel Ice Sheet Model (PISM-PIK) – Part 1: Model description, The Cryosphere, 5, 715–726, https://doi.org/10.5194/tc-5-715-2011, 2011.

Wyard, C.: Evaluation de la pertinence du couplage entre le modèle de circulation régionale MAR, et le modèle de calotte glaciaire GRISLI, sur le Groenland, 2015.